Time Reversed Absorbing Conditions (TRAC) in the Time and Frequency Domains

Franck Assous
Department of Mathematics
Bar-Ilan University
& Ariel Center University
Israel
franckassous@netscape.net

Marie Kray*
UPMC Université Paris 6
Laboratoire J.L. Lions
75005 Paris, France
kray@ann.jussieu.fr

Frédéric Nataf
UPMC Université Paris 6
Laboratoire J.L. Lions
75005 Paris, France
nataf@ann.jussieu.fr

Eli Turkel
School of Mathematical Sciences
Tel-Aviv University
69978 Ramat Aviv, Israel
turkel@math.tau.ac.il

ABSTRACT

We introduce the time reversed absorbing conditions ($TRAC$) in time reversal methods. These new boundary conditions enable one to "recreate the past" without knowing the source that has emitted the signals that are back-propagated. This new method does not rely on any *a priori* knowledge of the physical properties of the inclusion. We prove an energy estimate for the resulting non-standard boundary value problem. Numerical tests are presented in two dimensions for the wave and the Helmholtz equation. In particular the $TRAC$ method is applied to the differentiation between a single inclusion and a two close inclusion case. This technique is fairly insensitive with respect to noise in the data.

1. INTRODUCTION

Since the seminal paper by Fink et al. [13], time reversal is a subject of active research. The main idea is to take advantage of the reversibility of wave propagation phenomena such as it occurs in acoustics, elasticity or electromagnetism in a non dissipative unknown medium to back-propagate signals to the sources that emitted them. The initial experiment, see [13], was to refocus very precisely a recorded signal after passing through a barrier consisting of randomly distributed metal rods. The remarkable feature of this experiment is the concrete possibility to focus precisely a signal after it has crossed random barriers and even without knowing its location. There have been numerous applications of this physical principle, see [12] and references therein. First mathematical analyses can be found in [5] and [8].

An interesting possibility is to "recreate the past" in a medium from time-reversed boundary measurements. As shown experimentally in [11], it is necessary to know the source that emitted the signals to overcome the diffraction limit. The same difficulty was pointed out in [14] when numerically studying the initial instants of an earthquake by sending back long period time-reversed seismograms.

In this paper, we introduce a new method that enables to "recreate the past" without knowing the source which has emitted the signals that will be back-propagated. This is made possible by introducing time reversed absorbing conditions ($TRAC$) at the expense of removing a small region enclosing the scatterer. This technique will have at least two applications in inverse problems: the reduction of size of the computational domain and the determination of the location and volume of an unknown inclusion from boundary measurements.

The outline of the paper is as follows. We first introduce the principle of the $TRAC$ method in the time dependent domain. We then prove a related energy estimate. Afterward we introduce the principle of the $TRAC$ method in the time harmonic domain. We finally apply the $TRAC$ method to the differentiation between a single inclusion and two close inclusions in the partial aperture case. Hard, soft and penetrable inclusions are treated in the same way.

2. TIME REVERSED ABSORBING CONDITIONS

We consider an incident wave u^I impinging on an inclusion D characterized by physical properties different from the surrounding medium which is assumed to be homogeneous, $c = c_0$ in $\mathbb{R}^3 \setminus D$. The total field u^T can be decomposed

*Marie Kray presented this work to the 1st International ICST Workshop on New Computational Methods for Inverse Problems in May 16, 2011, École Normale Supérieure de Cachan (South of Paris), France.

NCMIP 2011, May 25, Paris, France

DOI 10.4108/icst.valuetools.2011.245812

into the incident and scattered fields, so $u^T := u^I + u^S$. We consider the problem in three dimensions and assume that the total field satisfies the linear wave equation

$$\frac{\partial^2 u^T}{\partial t^2} \; - \; c^2 \Delta u^T \; = \; 0 \qquad \text{in } (0, T_f) \times \mathbb{R}^3 \tag{1}$$

together with zero initial conditions. The scattered field u^S satisfies a radiation condition at infinity. Let Γ_R be a surface that defines a bounded domain Ω and encloses the inclusion D (see Figure 1). We assume that the incident wave u^I is generated by a point source such that after a time T_f the total field u^T is negligible in the bounded domain Ω. The total field u^T is recorded on Γ_R on the time interval $[0, T_f]$. Let $u_R^T := u^T(T_f - t, \vec{x})$ denote the total time reversed field that satisfies the physical equation (1). Similar definitions will be used for the incident and scattered fields.

Our aim is to reconstruct the time reversed field u_R^T from the measurements on Γ_R. For this purpose, we derive a boundary value problem (BVP), the solution of which is u_R^T. We know neither the physical properties nor the exact location of the inclusion D. The only things we know are the physical properties of the surrounding medium. Therefore, we introduce B a subdomain enclosing the inclusion D. Then we have to determine a specific boundary condition for u_R^T on the boundary ∂B so that the solution to this problem coincides with u_R^T in the restricted domain $\Omega \setminus B$.

In order to derive this boundary condition, we note that u^I satisfies (1) with $c = c_0$ the sound speed of the surrounding medium in $\mathbb{R}^3$, i.e. without any inclusion D, so that the scattered wave u^S also satisfies (1) but only in $\mathbb{R}^3 \setminus D$, with a Sommerfeld radiation condition at infinity with homogeneous initial conditions.

We look for a condition satisfied by u^S on ∂B. Absorbing boundary conditions (ABC) e.g. [6] construct accurate approximations to a perfectly absorbing boundary condition. We denote by ABC an absorbing boundary condition, that we choose to be the Bayliss-Turkel first order boundary condition. We take for B a ball of radius ρ denoted B_ρ. Then we can reasonably assume that

$$\text{ABC}(u^S) \; := \; \frac{\partial u^S}{\partial t} \; + \; c\frac{\partial u^S}{\partial r} \; + \; c\frac{u^S}{\rho} \; = \; 0 \text{ on } \partial B_\rho \tag{2}$$

where r is the radial coordinate with the origin at the center of the ball B_ρ. Our main ingredient is to "time reverse" this relation: using $u_R^S(t, \cdot) = u^S(T_f - t, \cdot)$, we get

$$-\frac{\partial}{\partial t}(u_R^S) \; + \; c\frac{\partial}{\partial r}(u_R^S) \; + \; c\frac{u_R^S}{\rho} \; = \; 0 \, .$$

Note that on ∂B_ρ, $\partial \, / \partial r = -\partial \, / \partial n$ where n is the outward normal to the restricted domain $\Omega \setminus B_\rho$. Multiplying by -1, we get the time reversed absorbing boundary condition TRAC:

$$\begin{array}{l} \text{TRAC}(u_R^S) \; := \\ \dfrac{\partial}{\partial t}(u_R^S(t, \cdot)) \; + \; c\dfrac{\partial}{\partial n}(u_R^S(t, \cdot)) \; - \; c\dfrac{u_R^S(t, \cdot)}{\rho} \; = \; 0 \, . \end{array} \tag{3}$$

Since $u_R^T = u_R^I + u_R^S$, we have $\text{TRAC}(u_R^T - u_R^I) = 0$ or equivalently $\text{TRAC}(u_R^T) = \text{TRAC}(u_R^I)$. The time reversed

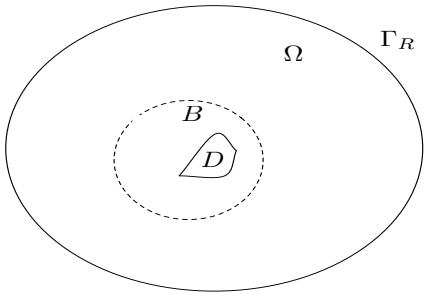

Figure 1: Geometry

problem analogous to (1) reads:

$$\left\{ \begin{array}{ll} \dfrac{\partial^2 u_R^T}{\partial t^2} - c^2 \Delta u_R^T = 0 & \text{in } (0, T_f) \times \Omega \setminus B_\rho \\ \text{TRAC}(u_R^T) = \text{TRAC}(u_R^I) & \text{on } \partial B_\rho \\ u_R^T(t, \vec{x}) = u^T(T_f - t, \vec{x}) & \text{on } \Gamma_R \\ \text{zero initial conditions.} & \end{array} \right. \tag{4}$$

The TRAC is not only not the standard BT^1 ABC but also has an "anti absorbing" term $(-cu_R^T/\rho)$. A natural concern arises about the well-posedness of BVP (4). Although we have not developed a general theory, we prove in section 3 an energy estimate for this problem in a special geometry. Moreover, in many computations we have never encountered stability problems.

The $TRAC$ method is also reliable if we work on the scattered field only and we are able to recreate the past of the scattered field. Indeed, the scattered field is the inclusion's response to the incident wave that impinged it. The time reversed problem for the scattered field reads:

$$\left\{ \begin{array}{ll} \dfrac{\partial^2 u_R^S}{\partial t^2} - c^2 \Delta u_R^S = 0 & \text{in } (0, T_f) \times \Omega \setminus B_\rho \\ \text{TRAC}(u_R^S) = 0 & \text{on } \partial B_\rho \\ u_R^S(t, \vec{x}) = u^S(T_f - t, \vec{x}) & \text{on } \Gamma_R \\ \text{zero initial conditions.} & \end{array} \right. \tag{5}$$

In what follows we present some numerical experiments. They all have been performed in two dimensions. In that case, the time-reversed absorbing condition becomes (see [3]):

$$\begin{array}{l} \text{TRAC}(u_R^S) \; := \\ \dfrac{\partial}{\partial t}(u_R^S(t, \cdot)) \; + \; c\dfrac{\partial}{\partial n}(u_R^S(t, \cdot)) \; - \; c\dfrac{u_R^S(t, \cdot)}{2\rho} \; = \; 0 \, . \end{array} \tag{6}$$

As a first test case, we consider an inclusion that is a soft disk and B_ρ is a disk of variable radius. Results are depicted on Figure 2, where we have three lines and several columns. Each line corresponds to a numerical time-reversed experiment and each column corresponds to a snapshot of the solution at a given time. The left column corresponds to the initial time for the time-reversed problem, equivalent to $t = T_f$ for the forward problem. The right column is the solution at the final time of the reversed simulation which

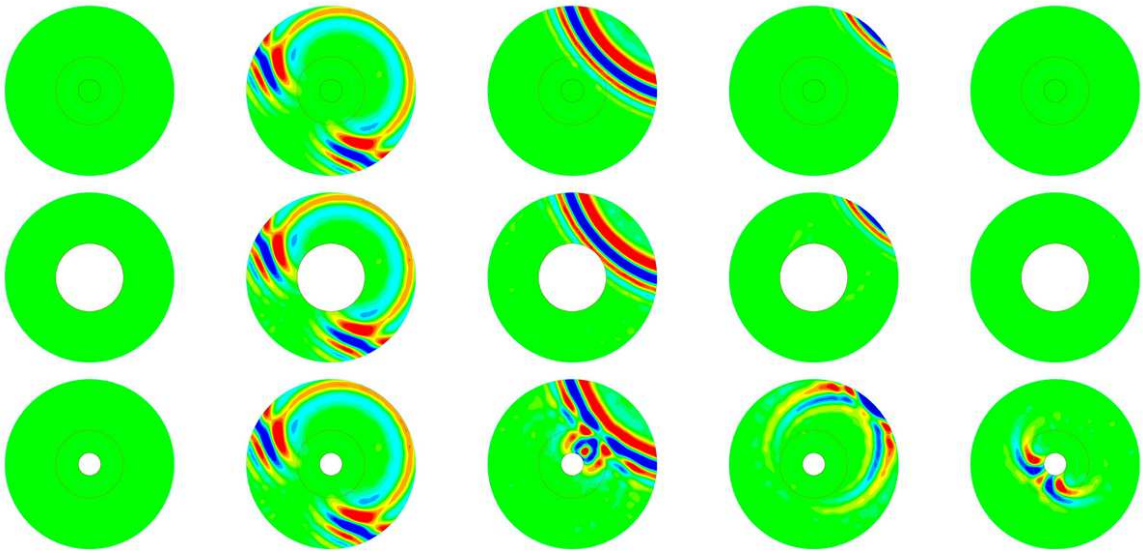

Figure 2: Time reversed solutions snapshots for a soft inclusion D: perfect time reversed (TR) solution on the upper line, TR solution for B_ρ enclosing D in the middle line and TR solution for B_ρ not enclosing D on the bottom line (final solution is not zero). The incident signal comes from top-right.

corresponds to the initial time $t = 0$ for the forward problem. In the top line, we display the perfect time reversed solution which is the reverse of the forward problem in the whole domain Ω. For the inverse problem, the data is not known. It is shown for reference only.

In the middle line, we display the solution of the reversed problem (4) with a ball B_ρ which encloses the inclusion. As expected, the sequence of snapshots is the restriction to the domain $\Omega \setminus B_\rho$ of the top line. This exemplifies one application of the *TRAC* method: if we know that the ball B_ρ encloses the inclusion we are able to reconstruct the signal in a region that is closer to the inclusion than the line of receivers Γ_R. This allows the reduction of the size of the computational domain. In this respect, the method is related to the redatuming method, see [7]. In the bottom line, we show the solution of the reversed problem (4) with a ball B_ρ smaller than the soft disk. In contrast to the previous case, the sequence of snapshots differs from the top line.

For the inverse problem of locating the scatterer, we only know that at the final time the solution should be zero. In the middle line, this criterion is satisfied and we can thus infer that the inclusion D is included in the ball B_ρ. On the other hand, when the final solution in the bottom line is not zero it shows that D is not included in the ball B_ρ. This observation leads to introduce an easy to compute criterion which is independent of the size of the domain:

$$J_{FT}(B_\rho) := \frac{\|u_R^S(T_f,\cdot)\|_{L^\infty(\Omega\setminus B_\rho)}}{\sup_{t\in[0,T_f]}\|u^I(t,\cdot)\|_{L^\infty(\Omega)}} \,. \tag{7}$$

Inverse problems are frequently ill-posed. Hence, a crucial question is the sensitivity of the method with respect to noise in the data. Therefore, we shall add Gaussian noise by replacing the recorded data u^S on Γ_R by

$$u^S_{\text{Noise}} := (1 + \mathit{Coeff} \times \texttt{randn})\, u^S \,, \tag{8}$$

Table 1: Results of the criterion $J_{FT}(B_\rho)$ (7) for different levels of noise on the recorded data.

Noise level	$D \subset B_\rho$	$D \not\subset B_\rho$
0%	1.40%	51.94%
10%	3.22%	51.51%
20%	7.18%	52.00%
30%	11.97%	54.69%
50%	14.49%	58.55%

where `randn` satisfies a centered reduced normal law and *Coeff* is the level of noise. The results of the final time criterion (7) are presented in Table 1. The level of noise is between 0% and 50%. We can discriminate between the case where the ball contains or does not contain the inclusion D up to 50% noise. Thus, the method *TRAC* appears to be relatively insensitive to noise on the recorded data.

3. ENERGY ESTIMATE

A natural concern arises about the well-posedness of *BVP* (4). Hence we propose an energy estimate in a particular geometry to prove the well-posedness of the *TRAC* method.

PROPOSITION 3.1. – *Let the trial subdomain B_ρ be a ball of radius ρ, and denote by r the radial coordinate with the origin at the center of B_ρ. Let g be a real-valued function on ∂B_ρ and u satisfy the following equations (see Figure 1):*

$$\begin{cases} \dfrac{\partial^2 u}{\partial t^2} - c^2\Delta u = 0 & \text{in } \Omega\setminus B_\rho \\ u = 0 & \text{on } \Gamma_R \\ \dfrac{\partial u}{\partial t} + c\left(\dfrac{\partial u}{\partial n} - \dfrac{u}{\rho}\right) = g & \text{on } \partial B_\rho \\ u = u_0 \text{ and } \dfrac{\partial u}{\partial t} = u_1 & \text{at } t = 0\,. \end{cases} \tag{9}$$

If Ω is a ball of radius R concentric to B_ρ, we have the following energy estimate written for the BVP (9) *in spherical coordinates (r,θ,ϕ):*

$$\begin{aligned}&\frac{1}{2}\frac{d}{dt}\left[\iiint r^2\sin\phi\,(\frac{\partial u}{\partial t})^2+c^2\sin\phi(\frac{\partial(ru)}{\partial r})^2\right.\\&\left.+c^2\sin\phi(\frac{\partial u}{\partial\phi})^2+\frac{c^2}{\sin\phi}(\frac{\partial u}{\partial\theta})^2\right]\\&+\iint_{r=\rho}c\rho^2\sin\phi(\frac{\partial u}{\partial t})^2\\&=\iint_{r=\rho}c\rho^2\sin\phi\,\frac{\partial u}{\partial t}\,g\ .\end{aligned}\tag{10}$$

Remark 1. – *The energy estimate* (10) *is not the standard energy estimate because of the term $(\partial(ru)/\partial r)^2$. We get this term by using an equivalent formulation of the Laplacian in spherical coordinates, as explicited in the proof. This energy estimate proves the well-posedness of the* TRAC *method but is not physically interpretable.*

Proof.
The Laplacian in spherical coordinates has the following expression:

$$\Delta=\frac{1}{r^2}\frac{\partial}{\partial r}(r^2\frac{\partial}{\partial r})+\frac{1}{r^2\sin^2\phi}\frac{\partial^2}{\partial\theta^2}+\frac{1}{r^2\sin\phi}\frac{\partial}{\partial\phi}(\sin\phi\frac{\partial}{\partial\phi})\ .\tag{11}$$

The energy estimate is based on an equivalent formulation of the Laplacian in spherical coordinates:

$$\Delta=\frac{1}{r}\frac{\partial^2}{\partial r^2}(r\,\cdot)+\frac{1}{r^2\sin^2\phi}\frac{\partial^2}{\partial\theta^2}+\frac{1}{r^2\sin\phi}\frac{\partial}{\partial\phi}(\sin\phi\frac{\partial}{\partial\phi})\ .$$

We multiply (9) by $\partial u/\partial t$ and integrate by parts (recall the volume element is $r^2\sin\phi\,dr\,d\theta\,d\phi$). We detail the computation for the term arising from the radial derivative since it is the only non classical one. We have:

$$\begin{aligned}&-\iiint\frac{c^2}{r}\frac{\partial^2}{\partial r^2}(r\,u)\frac{\partial u}{\partial t}\,r^2\sin\phi\,dr\,d\theta\,d\phi\\&=\iiint c^2\frac{\partial(r\,u)}{\partial r}\frac{\partial^2(r\,u)}{\partial r\partial t}\sin\phi\,dr\,d\theta\,d\phi\\&-\left[\iint c^2\frac{\partial(r\,u)}{\partial t}\frac{\partial(r\,u)}{\partial r}\sin\phi\,d\theta\,d\phi\right]_{r=\rho}^{r=R}\ .\end{aligned}$$

Thanks to the homogeneous Dirichlet condition on Γ_R, the normal derivative on Γ_R vanishes. Thus we focus on the boundary term at $r=\rho$:

$$\begin{aligned}&\iint_{r=\rho}c^2\frac{\partial(r\,u)}{\partial t}\frac{\partial(r\,u)}{\partial r}\sin\phi\,d\theta\,d\phi\\&=\iint_{r=\rho}c\rho\frac{\partial(r\,u)}{\partial t}c\,(\frac{\partial u}{\partial r}+\frac{u}{\rho})\sin\phi\,d\theta\,d\phi\ .\end{aligned}$$

Since at $r=\rho$, $\partial/\partial r=-\partial/\partial n$ we have using (9):

$$\begin{aligned}&\iint_{r=\rho}c\rho\frac{\partial(r\,u)}{\partial t}c\,(\frac{\partial u}{\partial r}+\frac{u}{\rho})\sin\phi\,d\theta\,d\phi\\&=\iint_{r=\rho}c\rho\frac{\partial(r\,u)}{\partial t}\left(\frac{\partial u}{\partial t}-g\right)\sin\phi\,d\theta\,d\phi\\&=\iint_{r=\rho}c\rho^2(\frac{\partial u}{\partial t})^2\sin\phi\,d\theta\,d\phi-\iint_{r=\rho}c\rho^2\frac{\partial u}{\partial t}g\sin\phi\,d\theta\,d\phi\ .\end{aligned}$$

By rewriting the second member in the other side of the equation, we find the energy estimate (10). ■

A similar result can also be found in [4] with an absorbing boundary condition on the external border.

4. THE *TRAC* METHOD IN THE HARMONIC CASE

We consider the time-harmonic counterpart of the problem (1) and we denote by ω the dual variable of t for the Fourier transform in time. The unknown total field $\hat{u}^T$ is decomposed into the sum of an incident field $\hat{u}^I$ and a scattered field $\hat{u}^S$. The Helmholtz problem is:

$$-\omega^2\hat{u}^T-c^2\Delta\hat{u}^T\ =\ 0\tag{12}$$

with the scattered field $\hat{u}^S$ satisfying a Sommerfeld condition at infinity. As in the time-dependent case, we introduce a surface Γ_R that defines a bounded domain Ω (see Figure 1).

Let $\hat{v}$ be a field that satisfies the harmonic equation (12). We denote by $\hat{v}_R$ the corresponding harmonic time-reversed field that still satisfies the same equation. Let $v(t,\vec{x})$ be a time dependent real valued function, solution to the wave equation, and $v_R(t,\vec{x}):=v(-t;\vec{x})$ its associated time-reversed function. Since we consider the harmonic case, there is no notion of time t. Thus the Fourier transform in time of the above definition becomes:

$$\begin{aligned}\hat{v}_R(\omega,\vec{x})\ &=\ \int v(-t,\vec{x})e^{-i\omega t}dt\\&=\ \int v(t,\vec{x})e^{i\omega t}dt\\&=\ \overline{\int v(t,\vec{x})e^{-i\omega t}dt}\\&=\ \overline{\hat{v}}(\omega,\vec{x})\ .\end{aligned}$$

This identity shows that phase conjugation is the extension of the Fourier transform of the time-reversal process in the case of the Helmholtz equation. This relation is the basis of phase conjugation in synthetic aperture radar (SAR), see [10]. Like in the time dependent case, the time-reversed total field $\hat{u}_R^T$ satisfies the time reversed problem in the reduced domain $\Omega\setminus B_\rho$:

$$\begin{cases}-\omega^2\hat{u}_R^T-c^2\Delta\hat{u}_R^T=0 & \text{in }\Omega\setminus B_\rho\\ \mathrm{TRAC}(\hat{u}_R^T)=\mathrm{TRAC}(\overline{\hat{u}^I}) & \text{on }\partial B_\rho\\ \hat{u}_R^T=\overline{\hat{u}^T} & \text{on }\Gamma_R\end{cases}\tag{13}$$

where the boundary condition TRAC becomes:

$$\mathrm{TRAC}(\hat{u}_R^S):=i\omega\hat{u}_R^S+c\frac{\partial\hat{u}_R^S}{\partial n}-\frac{c\hat{u}_R^S}{\rho}\ .\tag{14}$$

Here again the time-reversed absorbing condition TRAC is not the BT^1 absorbing boundary condition, because of an "anti absorbing" lower order term.

We present numerical tests in the time-harmonic case. An illustration is proposed in Figure 3 in the case of a soft square shaped inclusion D. The picture is composed as follow: On the top left figure we plot the modulus of the total field $|u^T|$ which coincides with the modulus of its conjugate field $|\bar{u}^T|$. On the right, we display the field obtained by the phase conjugation method by solving the classical phase conjugation

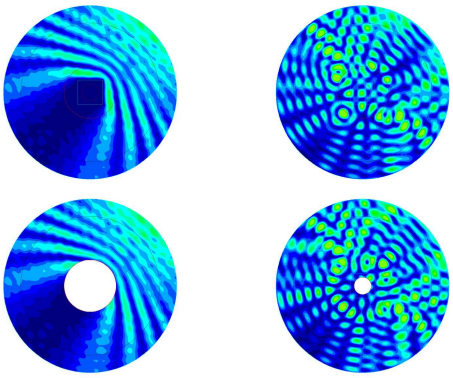

Figure 3: Phase conjugation for a soft square shaped inclusion of length $2\,\lambda$. From left to right, from top to bottom : perfect, phase conjugation, *TRAC* with a ball enclosing the inclusion, *TRAC* with a ball inside the inclusion.

problem (15):

$$\begin{cases} -\omega^2 \hat{u}_R^T - c^2 \Delta \hat{u}_R^T = 0 & \text{in } \Omega \\ \hat{u}_R^T = \overline{\hat{u}^T} & \text{on } \Gamma_R \,. \end{cases} \tag{15}$$

We see that there is a large difference between the total field and the field reconstructed by the phase conjugation method. The two bottom figures illustrate the *TRAC* method. On the left figure, the ball encloses the square and the computed field is the restriction of the total field. On the right figure, the ball is inside the square and the computed field is very different from the total field.

In practice, we don't know the total field and we have to introduce a way to measure whether the artificial ball encloses the inclusion or not. In contrast to the time dependent case, we cannot use the criterion defined in (7) since in the harmonic case, there is no time and thus no final time. For this purpose, we introduce a new criterion derived from the use of absorbing boundary conditions. Indeed, the basis of the method is that the phase conjugated scattered field satisfies (14) at any point outside the inclusion. In equation (13) this relation is used on the boundary of the artificial ball B_ρ. Since u^T is computed numerically and u^I is given data, they are easily available at any point in $\Omega \setminus B_\rho$ and equation (14) can be computed at any point in $\Omega \setminus B_\rho$. Thus, following the principle of the *TRAC* method, we introduce a new boundary $\Gamma_{J_{\text{ABC}}}$, concentric to the artificial ball B_ρ, to design a new criterion:

$$J_{\text{ABC}}(B_\rho, \Gamma_{J_{\text{ABC}}}) := \frac{\left\| \text{TRAC}(\hat{u}_R^T - \overline{\hat{u}^I}) \right\|_{L^\infty(\Gamma_{J_{\text{ABC}}})}}{\left\| \text{TRAC}(\overline{\hat{u}^I}) \right\|_{L^\infty(\Gamma_{J_{\text{ABC}}})}} \,, \tag{16}$$

The results of the criterion are 6.34% when B_ρ encloses D versus 69.18% if not. Note that we do not have 0% in the case $D \subset B_\rho$ because of the approximate absorbing boundary condition. Nevertheless we are able to discriminate the two cases.

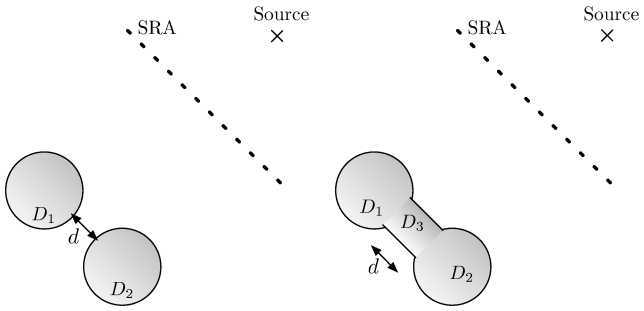

Figure 4: (a) Configuration for two distinct close inclusions D_1 and D_2. (b) Configuration for a single inclusion $D_1 \cup D_2 \cup D_3$.

5. ONE SINGLE INCLUSION VS TWO CLOSE INCLUSIONS

The aim of this part is to investigate the ability of the *TRAC* method to discriminate between a single inclusion and two distinct close inclusions. This test is inspired by a more realistic setting. First we now use a source-receiver array (SRA) with partial aperture and discrete transducers, whereas in the previous case, the SRA has a full aperture and even continuous transducers. Then our intent is to detect one or two iron or plastic mines in a background medium made of sand. The physical equation we use is a scalar wave equation derived from the Maxwell equations, as proposed in [1]:

$$\varepsilon \frac{\partial^2 u}{\partial t^2} - \text{div}\left(\frac{1}{\mu}\nabla u\right) = 0 \,, \tag{17}$$

with the electric permittivity ε and the magnetic permeability μ of the medium, the speed c satisfying $c^2 = (\varepsilon\mu)^{-1}$. Both of these parameters can be expressed with an absolute value multiplied by a relative value

$$\begin{aligned} \varepsilon &= \varepsilon_0 \varepsilon_r \\ \mu &= \mu_0 \mu_r \,, \end{aligned}$$

where ε_0 and μ_0 are the electromagnetic constants of the vacuum. As for the background and the mines, we consider parameters chosen as follows

	sand	iron mine	plastic mine
ε_r	3	1	1.5
μ_r	1	10,000	1

Globally the iron mine acts like a "hard" inclusion, with a velocity ratio close to zero, whereas the plastic mines are penetrable inclusions with a ratio velocity of $\sqrt{2}$, so close to 1. In this paper, we only present the results for the plastic mines. Similar results about iron mines are listed in [2].

As depicted in Figure 4, we denote by D_1 and D_2 the two close inclusions and by $D_1 \cup D_2 \cup D_3$ the single inclusion consisting of D_1 and D_2 connected by D_3. Inclusions D_1 and D_2 are balls of radius λ, where λ is the wavelength. Moreover the connection D_3 has a thickness of λ and a length d which can be $3\lambda/2$ or $\lambda/2$. A more detailed description of the configuration can be found in [2].

As expected, in the partial aperture case we cannot use the final time criterion J_{FT} (7). Due to the use of an artificial

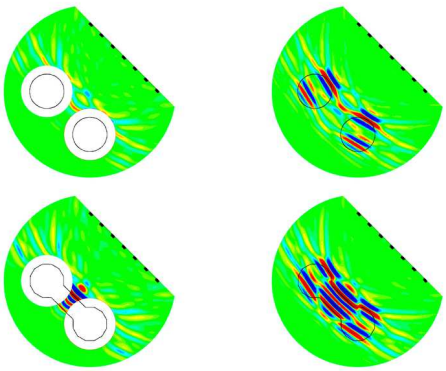

Figure 5: Imaging function (18) **for distant plastic mines,** $d = 3\lambda/2$**.**

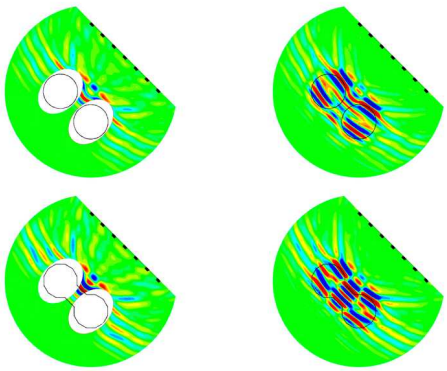

Figure 6: Imaging function (18) **for close plastic mines,** $d = \lambda/2$**.**

boundary condition on the external boundary not equipped with receivers, the signal vanishes at the final time whether or not B_ρ encloses D. We introduce a new criterion inspired from reverse time migration techniques, see [9]. It consists in cross-correlating the incident field u^I with the time reversed scattered field u_R^S. In classical applications of earth imaging, the following integral is computed as a function of $\vec{x} \in \Omega$

$$f(\vec{x}) := \int_{t=0}^{t=T_f} v_R^S(T_f - t, \vec{x}) \times u^I(t, \vec{x})\ dt\,. \qquad (18)$$

The function f images the discontinuities of the propagation speed $c(\vec{x})$, see [9]. The new cross-correlation criterion reads:

$$J_{CC}(B_\rho) \ := \ \frac{\left\| \int_{t=0}^{t=T_f} u_R^S(T_f - t, .) \times u^I(t, .)\ dt \right\|_{L^\infty(\Omega \setminus B_\rho)}}{\left\| \int_{t=0}^{t=T_f} |u^I(t, .)|^2\ dt \right\|_{L^\infty(\Omega)}}\,, \qquad (19)$$

where u_R^S is the solution to problem:

$$\begin{cases} \varepsilon \dfrac{\partial^2 u_R^S}{\partial t^2} - \operatorname{div}\left(\dfrac{1}{\mu} \nabla u_R^S\right) = 0 & \text{in } (0, T_f) \times \Omega \setminus B_\rho \\ \operatorname{TRAC}(u_R^S) = 0 & \text{on } \partial B_\rho \\ u_R^S(t, \vec{x}) = u^S(T_f - t, \vec{x}) & \text{on } \Gamma_R \\ \operatorname{ABC}(u_R^S) = 0 & \text{on } \partial\Omega \setminus \Gamma_R \\ \text{zero initial conditions.} \end{cases} \qquad (20)$$

When trial domain B_ρ encloses inclusion D, there is no discontinuity to be imaged in $\Omega \setminus B_\rho$ and the criterion $J_{CC}(B_\rho)$ should be small. At the opposite, when part of inclusion D is outside B_ρ, we note that the function f images this part, so that J_{CC} should be significantly larger. In order to get comparable figures, for a trial domain B_ρ instead of $J_{CC}(B_\rho)$ defined in (19), we introduce a relative criterion, in the same spirit as the signal-to-noise ratio (SNR),

$$J_{CC}^{rel}(B_\rho) := \frac{J_{CC}(\emptyset)}{J_{CC}(B_\rho)}\,, \qquad (21)$$

where $J_{CC}(\emptyset)$ is the cross-correlation criterion computed in absence of any trial domain B_ρ, similarly to the classical approach in time reversal techniques. Note that in this case, criterion $J_{CC}(\emptyset)$ should be large. Consequently, when $J_{CC}^{rel}(B_\rho)$ is close to one, we infer that the domain B_ρ does not enclose the inclusion. In the opposite case, we can reasonably assume that when $J_{CC}^{rel}(B_\rho)$ is large, trial domain B_ρ encloses inclusion D.

On Figure 5, we plot the values of the function f defined in equation (18) for $d = 3\lambda/2$. The first row corresponds to two distinct inclusions whereas the second row deals with a single inclusion. The right column corresponds to the classical case where $B_\rho = \emptyset$. In the left column, we use a trial domain B_ρ made of two connected components. When there is no trial domain, the cross-correlation function f images decently the illuminated edges of the inclusions. Pictures on the left column illustrate the principle of the $TRAC$ method. As expected, when trial domain B_ρ encloses the inclusions (top left picture), there is nearly no image. Otherwise, the illuminated edge of the part of the inclusion which is not embedded in B_ρ is correctly imaged (bottom left picture). Thus we are able to distinguish between one inclusion and two close ones.

Figure 6 represents the same configuration but for a smaller d equals to $\lambda/2$. When there is no trial domain (right column), the imaging function f is not able to distinguish two inclusions (top right) from one inclusion (bottom right), due to the proximity of the inclusions. On the contrary when trial domain B_ρ encloses the inclusions (top left), the function f is significantly smaller than in the case where B_ρ leaves part of the inclusion (part of D_3) on the outside (bottom left picture). Note that due to the proximity of the inclusions, we have used trial domains made of two ellipses.

Table 2 presents the results of the relative cross-correlation criterion for plastic mines when the two distinct inclusions are close ($d = \lambda/2$) and distant ($d = 3\lambda/2$). The two left columns describe the trial ball configuration and the level of noise. The two middle columns represent the values of the relative cross-correlation criterion (21) in the case of two distant inclusions, and the two right colums, the values of the criterion in the case of two close inclusions. Each configuration of trial ball was treated for several levels of noise. The first trial domain B_ρ (four first lines after the header) is an ellipse that encloses all the inclusion(s). The results of the criterion are significantly large to assert that we correctly enclose the inclusion(s). On the contrary, the four middle lines are considering a trial domain B_ρ that

Table 2: Relative cross-correlation criterion J_{CC}^{rel} values to distinguish between one single inclusion and two distinct inclusions. Results for plastic distant inclusions ($d = 3\lambda/2$) and plastic close inclusions ($d = \lambda/2$), and for different levels of noise.

		$d = 3\lambda/2$		$d = \lambda/2$	
Trial Domain	Noise level	2 inclusions	1 inclusion	2 inclusions	1 inclusion
 $D \subset B_{ellipse}$	0%	4.68	7.00	8.13	9.49
	10%	4.68	7.04	8.22	9.49
	20%	4.66	7.00	8.43	9.56
	30%	4.77	7.33	8.33	9.57
 $D_2 \not\subset B$	0%	0.94	0.88	0.92	0.91
	10%	0.95	0.88	0.92	0.91
	20%	0.93	0.88	0.92	0.92
	30%	0.94	0.89	0.91	0.92
 $D_3 \not\subset B$	0%	4.88	0.92	3.36	1.55
	10%	4.89	0.92	3.33	1.54
	20%	4.91	0.93	3.32	1.55
	30%	4.54	0.92	3.34	1.56

only encloses D_1. So the function f images D_2 and, when it exists, D_3. In this configuration, we have results of the criterion close to 1, as expected because we are wrong in the detection of all the inclusions. Finally, the four bottom lines are presenting the results of the criterion in the case of a two connected components trial ball. For distant inclusions, we can discriminate easily between a single inclusion and two distinct inclusions, thanks to large values of J_{CC}^{rel} in the third column and values close to 1 in the fourth column. On the other hand, the two right columns ($d = \lambda/2$) indicate that it is more difficult but still possible to distinguish between one inclusion and two close inclusions.

6. CONCLUSION

We have introduced the time reversed absorbing conditions (*TRAC*). They enable to "recreate the past" without knowing the source which has emitted the signals that are back-propagated. This is made possible at the expense of removing a small region enclosing the scatterer. Applications to inverse problems are presented:

1. the reduction of size of the computational domain by redefining the reference surface on which the receivers appear to be located;
2. the determination of the location of an unknown inclusion from boundary measurements.

We stress the fact that in contrast to many methods in inverse problems, the *TRAC* method does not rely on any *a priori* knowledge of the physical properties of the inclusion. Hard, soft and penetrable inclusions are treated in the same way. In [3], the feasibility of the method is shown for both time-dependent and harmonic equations (acoustics and electromagnetism) and in [2], the method is applied in partial aperture case for a more realistic case. Moreover, the method is shown to be very robust with respect to noisy data.

7. REFERENCES

[1] H. Ammari, E. Iakovleva, and D. Lesselier. A MUSIC algorithm for locating small inclusions buried in a half-space from the scattering amplitude at a fixed frequency. *Multiscale Modeling and Simulation*, 3(3):597–628, 2005.

[2] F. Assous, M. Kray, and F. Nataf. Time Reversed Absorbing Condition in the Partial Aperture Case. http://hal.archives-ouvertes.fr/hal-00581291/en/, submitted.

[3] F. Assous, M. Kray, F. Nataf, and E. Turkel. Time reversed absorbing condition: Application to inverse problem. http://hal.archives-ouvertes.fr/hal-00491912/fr/, to appear in Inverse Problem.

[4] F. Assous, M. Kray, F. Nataf, and E. Turkel. Time reversed absorbing conditions. *Comptes Rendus Mathematiques*, 348(19-20):1063–1067, 2010.

[5] C. Bardos and M. Fink. Mathematical foundations of the time reversal mirror. *Asymptot. Anal.*, 29(2):157–182, 2002.

[6] A. Bayliss and E. Turkel. Radiation boundary conditions for wave-like equations. *Comm. Pure Appl. Math.*, 33(6):707–725, 1980.

[7] J. Berryhill. Wave-equation datuming. *Geophysics*, 44(206):132944, 1979.

[8] P. Blomgren, G. Papanicolaou, and H. Zhao. Super-resolution in time-reversal acoustics. *J. Acoust. Soc. Am.*, 111:230–248, 2002.

[9] J. F. Claerbout. *Imaging the Earth's interior*. Blackwell, 1985.

[10] J. Curlander and R. McDonough. *Synthetic Aperture Radar*. Wiley, 1991.

[11] J. de Rosny and M. Fink. Overcoming the diffraction limit in wave physics using a time-reversal mirror and a novel acoustic sink. *Phys. Rev. Lett.*, 89 (12), 2002.

[12] M. Fink. *Renversement du temps, ondes et innovation*. Ed. Fayard, 2009.

[13] M. Fink, F. Wu, D. Cassereau, and R. Mallart. Imaging through inhomogeneous media using time reversal mirrors. *Ultrasonic Imaging*, 13(2):199 – 199,

1991.

[14] C. Larmat, J.-P. Montagner, M. Fink, Y. Capdeville, A. Tourin, and E. Clévédé. Time-reversal imaging of seismic sources and application to the great sumatra earthquake. *Geophys. Res. Lett.*, 33, 2006.